


Re–Os and Pb isotope features of pyrite in the Shihangli graphite deposit: implications of coal-generated graphite mineralization in central Hunan, South China

Yong Zhang¹  · Dongsheng Ma² · Jian-Feng Gao³ · Jiayong Pan¹ · Xupeng Lv⁴ · Guoqi Liu¹ · Fujun Zhong¹ · Xiaotian Zhang¹ · Ying Liu¹

Received: 1 October 2022 / Revised: 8 May 2023 / Accepted: 18 May 2023 / Published online: 14 June 2023

© The Author(s), under exclusive licence to Science Press and Institute of Geochemistry, CAS and Springer-Verlag GmbH Germany, part of Springer Nature 2023

Abstract The coal metamorphism in Central Hunan provides valuable information about hydrothermal activity and water/rock reactions. Learning how to collect age data on hydrothermal fluid systems is necessary for understanding the history and genetic mechanisms of large-scale coal-generated graphite deposits. The Shihangli graphite deposit, formed by significant siliceous hydrothermal alteration, is the most distinctive in Central Hunan. Re–Os dating of pyrite from the Shihangli graphite deposit demonstrates that the coal-generated graphite mineralization age is $\sim 127.6 \pm 3.8$ Ma. Based on *in-situ* mineral analysis, the hydrothermal pyrite in the Shihangli graphite deposit is mostly enriched in Sb, As, Au, W, Ag, Cu, Pb, and Zn. Based on the pyrite Re–Os isochron, the initial ($^{187}\text{Os}/^{188}\text{Os}$) values of pyrite were 1.03 ± 0.24 and the Os(t) values varied from 571.8 to 755.1. Pyrite from the Shihangli graphite deposit comprises a Pb isotope

composition similar to that of the Madiyi Formation bulk rock and stibnite from the Xikuangshan Sb deposit. Based on the Re–Os, Sr, S, and Pb isotopic compositions of sulfides in the graphite and Sb deposits in Central Hunan, the Madiyi Formation was likely the primary source of ore-forming elements (Sb, Au, and As). The Re–Os and Pb isotope compositions of pyrite most likely reflect when large-scale fluid migration and coal-generated graphite mineralization occurred in Central Hunan.

Keywords Pyrite · Re–Os · Pb isotope · Graphite · Central Hunan

✉ Jian-Feng Gao
gaojianfeng@mail.gyig.ac.cn

Yong Zhang
zhycy2004@163.com

Dongsheng Ma
dongsma@qq.com

Jiayong Pan
jypan@ecut.edu.cn

Xupeng Lv
175243732@qq.com

Guoqi Liu
liuguoqi@ecut.edu.cn

Fujun Zhong
zhongfujun@ecut.edu.cn

Xiaotian Zhang
xtzhangeology@163.com

Ying Liu
liuying@ecut.edu.cn

- 1 State Key Laboratory of Nuclear Resources and Environment, East China University of Technology, Nanchang 330013, China
- 2 School of Earth Sciences and Engineering, Nanjing University, Nanjing 210046, China
- 3 State Key Laboratory of Ore Deposit Geochemistry, Institute of Geochemistry, Chinese Academy of Sciences, Guiyang 550081, China
- 4 Yunnan Institute of Geological Survey, Kunming 650032, China

1 Introduction

The formation of hydrothermal deposits is attributed to the formation of ore-forming fluids. These fluids are usually required in large volumes to form a massive hydrothermal deposit. As a result of large-scale fluid movement, large-scale hydrothermal alteration occurs in coal measure strata that are extensively scattered throughout Central Hunan, leading to the creation of endogenetic metal deposits and regional hydrothermal alterations (Dai et al. 2022; Fu et al. 2020b; Li et al. 2022; Ma and Liu 1992; Zhao et al. 2021). The Ceshui Formation, a crucial coal measurement layer of the Middle and Lower Carboniferous eras in the Central Hunan province (Wang et al. 2012a), experiences coal metamorphism primarily due to regional magmatic–hydrothermal alteration (An et al. 2016; Bi 1998; Bi et al. 1996, 1997). Based on geochemical investigations of trace elements in coal mines, ore-forming elements such as Sb and Ag are notably concentrated in coal, with Sb concentrations up to 45 ppm (Ma et al. 2005). The Carboniferous and Permian occurrence horizons of these coal mines are located above the Sb deposit (Devonian). Thus, they may be linked to the fluid circulation mechanism that occurs across the basin and Sb mineralization during the Yanshanian (Ma et al. 2005). Over 60% of the land area of Central Hunan, which has hundreds of local coal deposits, is exploited by 40 state-owned coal companies. These deposits included over 90% anthracite (graphite) (He 2008; Mo et al. 2020; Zhang 1980). As water/rock interaction has influenced the mineralization characteristics of these deposits on a basin scale, the formation of coal-generated graphite deposits in Central Hunan is likely to result from a regional hydrothermal event. Therefore, the formation age and genetic mechanism of large-scale coal-generated graphite deposits in Central Hunan remain important topics. The Shihangli graphite deposit in the Lower Carboniferous Ceshui Formation is a crucial example of such a deposit, and the pyrite quartz vein in this deposit most likely contains geological and geochemical information on local basin-scale (metallogenic) fluid activity occurrences and graphite mineralization.

Pyrite and molybdenite Os isotopic properties have been widely used to research metallogenic genesis and track the origin of metallogenic components in hydrothermal deposits (Deng et al. 2016; Duan et al. 2017; Hnatyshin et al. 2015; Jiang et al. 2000; Li et al. 2015a). Additionally, Pb isotope ratio analysis is a powerful tool for exploring the ore genesis and the metallogenic material origins because it is unaffected by hydrothermal alteration or weathering (Akiska et al. 2013; Jemmali et al. 2013a, b; Shah et al. 2010). The Pb isotope compositions of pyrite can be used to determine the development of metallogenic

fluids in hydrothermal deposits and the source of ore-forming materials (Wang et al. 2017b; Yuan et al. 2018; Zhai et al. 2018, 2019; Zhang et al. 2016, 2018). The Re–Os and Pb isotope compositions of hydrothermal pyrite can help determine the hydrothermal alteration time and suggest the metallogenic material sources.

Recently, studies have focused on how the age of large-scale fluid movement is constrained and the regional strata modification age caused by substantial fluid movement to form large-scale coal-generated graphite deposits in Central Hunan, China. This study used laser-ablation inductively coupled plasma mass spectrometry (LA-ICP-MS) and inductively coupled plasma mass spectrometry (ICP-MS) to identify the date of large-scale coal-generated graphite deposits in Central Hunan.

2 Regional geology

The Jiangnan Orogenic Belt, one of the major polymetallic metallogenic belts in China, runs along the northern margin of the Cathaysia and Yangtze blocks (Li et al. 2009; Shu 2012; Shu et al. 1995). This belt has several ore deposits, the most significant of which are the Central Hunan Sb–Au–W ore region and coal-generated graphite deposit (Fig. 1). The Western Hunan ore deposit, situated in the Neoproterozoic basement outcrop area around Central Hunan, is an Sb–Au–W subzone that forms a part of the Central Hunan ore field, which is Pb–Zn–Sb–Au–Fe–W–Mn metallogenic. The succession of Proterozoic metamorphic and Lower Paleozoic clastic rocks around the basin shows that the Western Hunan Sb–Au–W subzone is an ancient basin (Xu et al. 2008).

Granites are most commonly found on the outskirts of Central Hunan. The Indosinian period, which occurred between 225 and 210 Ma, was the peak period of magmatic activity and tungsten mineralization. Many Indosinian W deposits, such as the Dalongxi W deposit (Zhang et al. 2014), Zhazixi Sb–W deposit (Wang et al. 2012b), and Muguayuan W deposit (Li et al. 2018b) (Fig. 1), were formed by Indosinian granitic plutons. The Middle and Late Jurassic granites, on the other hand, are ultra hypabyssal; for example, the acid dikes (fine-grained granite and pegmatite veins) of the Baimashan–Wangyunshan granite formed between 170 and 150 Ma (Chen et al. 2007; Zhang 2018).

The Longshan Sb–Au deposit, Xikuangshan Sb deposit, and alternating coal metamorphism are all strongly associated with Yanshanian magmatism (such as graphitization and silicification) (An et al. 2016; Fu et al. 2020a, 2016). The Xikuangshan Sb and Woxi Au–Sb–W deposits are two major metal resources in Central Hunan (Zhou et al. 2023b; Dai et al. 2022) (Fig. 1). The Xikuangshan Sb deposit is the

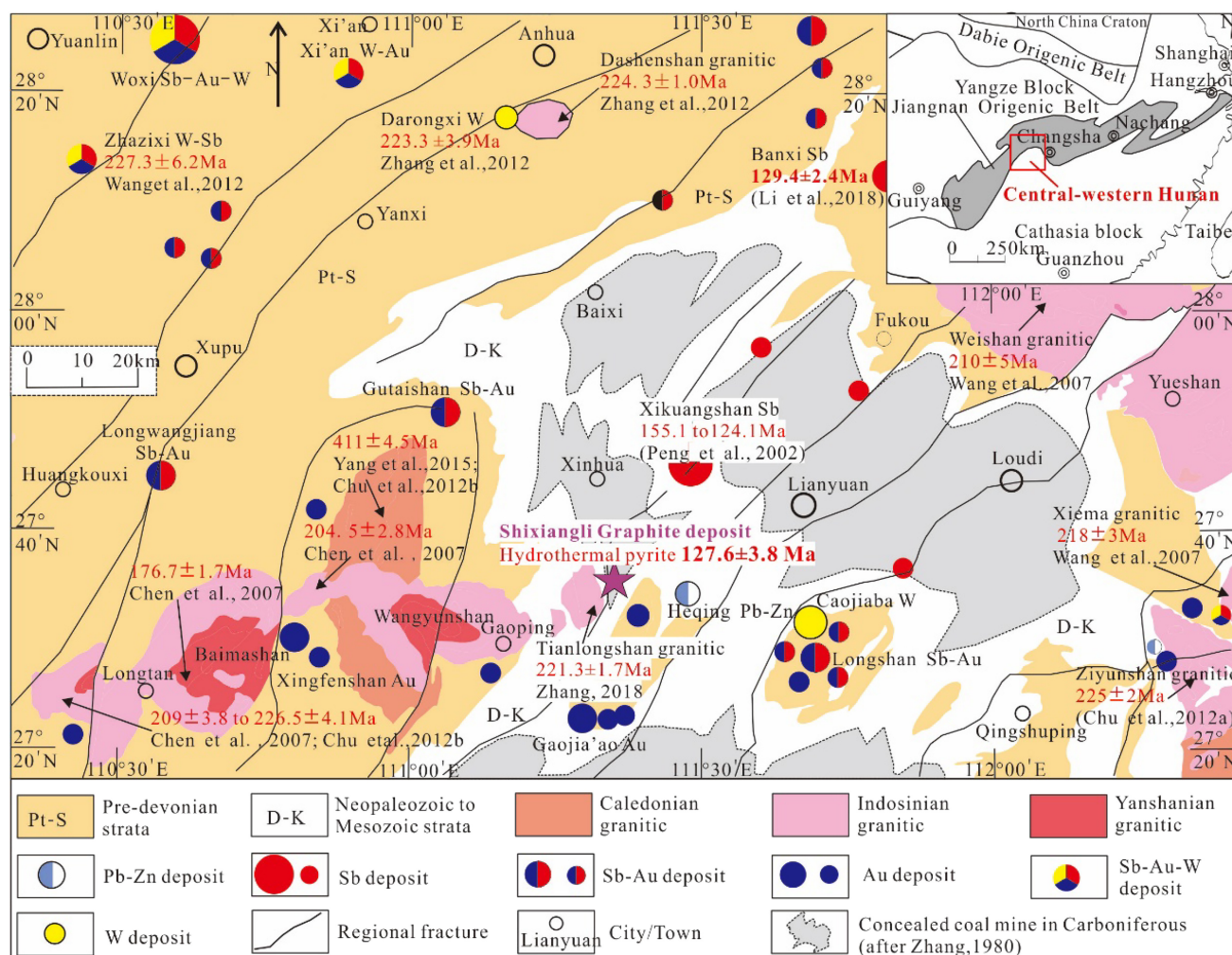


Fig. 1 Sketch map of the geology of Central Hunan Province in southern China (modified overall from Zhang et al. 2018c; Au deposits after Kang 2002, Sun et al. 2007, and Zhang et al. 2015; Sb and Sb–Au deposits after Ma et al. 2002)

largest Sb deposit globally, with more than 50% of the Sb produced and 2.5 Mt of total Sb metal reserves worldwide (Fu et al. 2020b; Hu et al. 2017; Laznicka 1999; Peng et al. 2003a; Yang et al. 2006b). The Upper Devonian black shale hosts the Xikuangshan Sb deposit (Fan et al. 2004), and the interlayer fault zones of silicified carbonates tightly limit orebodies, the bulk of which are stratiform. The primary stage of Sb mineralization is associated with significant silicic and carbonate alterations, resulting in a substantial silicified alteration halo surrounding Sb orebodies that are often limited by ore-forming fluids (Kuang 2000; Peng et al. 2003b; Yang et al. 2006a).

In the Early Carboniferous coal age, the Carboniferous Ceshui Formation is a notable coal-bearing deposit (He 2008). A major component of anthracite often undergoes significant thermal metamorphism in Carboniferous coal, transforming it into graphite ore (Li et al. 2013, 2017). The Shihangli graphite deposit in the Carboniferous Ceshui

Formation is an example of a coal-formed graphite deposit (Fig. 1).

3 Deposit geology

The Shihangli graphite deposit is situated in the Central Hunan province, ~ 1 km northeast of the Tianlongshan granitic pluton (221.3 ± 1.7 Ma) (Zhang 2018). This deposit is a metamorphic coal graphite deposit formed by regional hydrothermal alteration and has been mined since 1969 (Huang et al. 1985). The Lianyuan Coalfield is the major coal-producing region in the Hunan province. The overall architecture of the Shihangli mining zone resembles a roughly north–south syncline with asymmetric wings. The stratum is steep, partially upright, and occasionally inverted, with a well-preserved west wing of the syncline. The Tianlongshan granites are located to the west of the Shihangli mining zone. The granite intrusive strata range from

the Middle Devonian to the Lower Carboniferous systems, with biotite granodiorite and medium-grained (porphyritic) monzonite granite as the major lithologies. The coal and graphite ore have identical macroscopic features in terms of color and structure, but their hue of streaks differs. Graphite ore has a high density and a dazzling luster, and the fractures are cut or filled by fine quartz and calcite veins (Zhou et al. 2017).

The Shihangli deposit has a dip angle of 80° – 88° and a strike angle of 240° – 251° . The thickness of the graphite ore body ranges from 1 to 4 m, and the footwall and hanging wall of the deposit consist of sandstone to sandy mudstone (Fig. 2). The veined and stockwork quartz veins in the graphite ore body range from 1 to 20 cm in width. The frequency of quartz veins decreases as the distance between the graphite ore and the wall rock grows and the silicification and pyritization of the wall rock deteriorate. The silicified alteration zone is typically 1–10 m wide. Pure anthracite graphite ore has high conductivity and a steel-gray glass sheen (Fig. 3a). The strongly silicified wall rock has a pyritized vein of fine-grained banded quartz (Figs. 3b, c). Since its formation, the Ceshui Formation has undergone three stages of thermal change: deep-seated, regional, and hydrothermal fluid (Bi et al. 1996). The hydrothermal fluid developed quartz veins in the graphite ore when the coal seam was changed into a graphite ore body. Simultaneously, the rock on the top and lower walls experienced significant silicification-based changes. When the silicification of the rock surrounding the graphite ore continuously declines with distance, a hydrothermal alteration zone is generated (Fig. 3).

The Shihangli deposit comprises graphite ores with block, sheet, and strip structures. The graphite ore has a scaly crystalloblastic structure and is composed mainly of aphanitic graphite, quartz, mica, and pyrite (Figs. 3a, b).

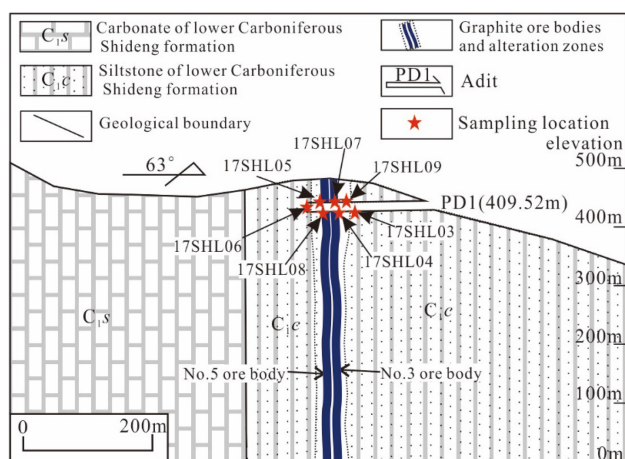


Fig. 2 Geological cross-section of the Shihangli graphite deposit (after Huang et al. 1985)

Based on the results of the chemical analysis, the fixed carbon mass fraction of graphite ore ranged from 64.4% to 87.7% (Mo et al. 2020; Zhou et al. 2017). Based on the research on trace elements in graphite ores, the principal impurity elements are Sb (50 ppm), Ag (61 ppm), and Au (0.04 ppm).

In this study, the Shihangli deposit was analyzed to determine its mineral paragenesis, which revealed the existence of three major stages of mineralization. Figure 4 summarizes the paragenetic sequence of the ore and gangue minerals in the Shihangli graphite deposit. Stage I of the stratiform graphite ore deposit comprises massive graphite and minor quartz mineralization (Fig. 3a). Subsequently, in Stage II, a silicification alteration characterized by significant quartz mineralization in a stratiform graphite ore body with minor pyrite, chalcopyrite, stibnite, and galena mineralization covered and changed this stage (Fig. 3b). Stage II was significantly cut and changed by Stage III, quartz–pyrite, which is distinguished by an assemblage of quartz, pyrite, and a small amount of calcite in quartz veins (Fig. 3c), which is covered by carbonation (stage IV).

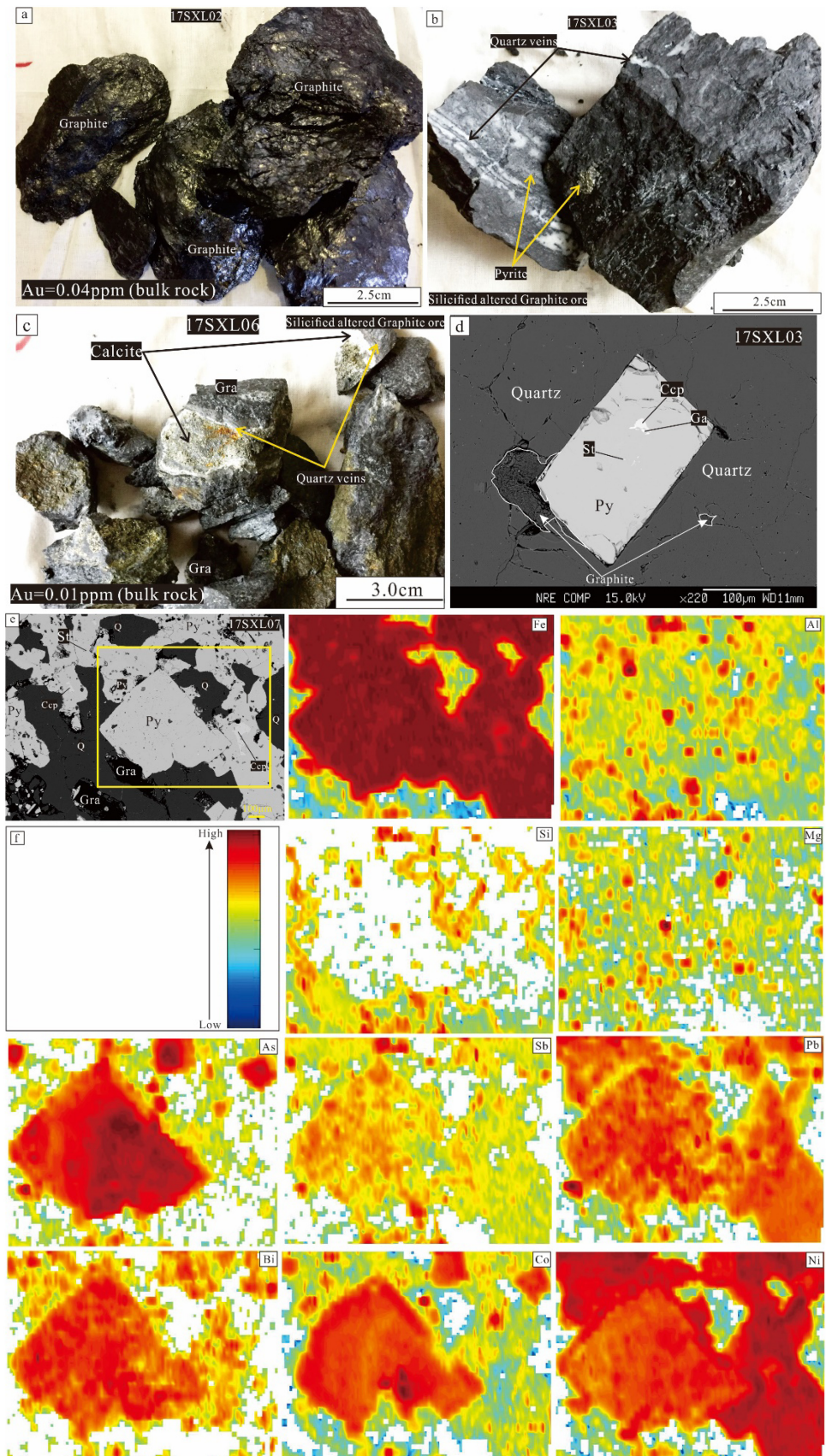
4 Samples and analytical methods

In this study, pyrite from the quartz vein in the Shihangli deposit was investigated (Fig. 3b and Table 1).

The State Key Laboratory of Nuclear Resources and Environment at the East China University of Technology in China uses a JEOL JXA-8230 electron microprobe to conduct quantitative chemical investigations on polished thin slices of pyrite. The operating settings were a probe current of 20 nA, a total acceleration voltage of 15 kV, and a pyrite beam diameter of 1 μm .

At Nanjing FocuMS Technology Co. Ltd., trace element studies of pyrite were conducted using an LA-ICP-MS on polished thin slices. The tests used a combination of the Teledyne Cetac Technologies Analyte Excite laser-ablation system (Bozeman, Montana, USA) and the Agilent Technologies 7700 \times quadrupole ICP-MS (Hachioji, Tokyo, Japan). A collection of beam delivery mechanisms homogenized the 193-nm ArF excimer laser before it was focused with a fluence of 6.06 J/cm^2 on the surface of minerals. A 44- μm spot with a 6-Hz repetition rate was used for the ablation treatment, which lasted 40 s (equating to 280 pulses). The ICP-MS-Data-Cal program used a 100% normalization method without using internal standards to achieve raw data reduction offline (Liu et al. 2008). Before each ablation, a 15-s gas background was collected, and spots with a diameter of 44 μm were ablated using an experimental technique at a repetition rate of 5 Hz for 40 s (equating to 240 pulses). Aerosol was efficiently

Fig. 3 Characteristics of graphite and pyrite in the Shihangli deposit: **a** graphite; **b** hydrothermal quartz veins; and **c, d** BSE images of pyrite grains and LA-ICP-MS maps of selected trace elements in pyrite from the Shihangli graphite deposit. Py-pyrite; Q-quartz; Ccp-copper



Stage	I	II	III	IV
Mineral	<i>Graphitization</i>	<i>Silicification</i>	<i>Quartz+sulfide</i>	<i>Carbonation</i>
Graphite	█			
Quartz		█	█	
Chalcopyrite			█	
Stibnite			█	
Pyrite		█	█	
Galana			█	
Calcite				█

Fig. 4 Mineral generation sequence of the Shihangli graphite deposit

transported by helium carrier gas, which was combined with argon via a T-connector before going into the ICP-MS. Sulfides were calibrated using synthetic basaltic glasses GSE-1G and USGS polymetallic sulfide pressed pellet MASS-1.

The trace element pyrite was mapped using LA-ICP-MS at Nanjing FocuMS Technology Co. Ltd. The spot diameter for the ablation technique was 44 μm at 10 Hz, the sample motion was in a straight line at 40 m/s, and the fluence was 3 J/cm^2 . Before and after sample analysis, background signals were gathered for around 30 s. The NIST 610 or GSE-1G external standard sample was evaluated for 40 s at the start and end of scanning the sample to be tested. Laboratory internal design software LIMS (based on MATLAB design) was used to process the data (Wang et al. 2017a; Xiao et al. 2018). The software automatically completed background removal and instrument signal drift during the whole analysis procedure.

The pyrite was selected under a binocular microscope to have a purity of more than 99% and then ground to 200 mesh in an agate bowl before Re–Os isotopic analysis. The samples from the pyrite quartz vein were crushed to a size of 60–80 mesh. The State Key Laboratory of Isotope Geochemistry at the Guangzhou Institute of Geochemistry in China conducted this analysis and additional tests where the materials were dissolved in a Carius tube. Re–Os isotope analysis principles and specific analytical steps were taken from previous studies (Shirey and Walker 1995; Li et al. 2014, 2015b).

The measurements of the pyrite lead isotopes were conducted at ALS Cemex (Guangzhou) Co. Ltd. using ICP-MS. The standard procedure was leaching with HCl on a hotplate after digesting 0.5 g of a prepared sample with four acids (HClO_4 , HF, HNO_3 , and HCl) until dry. The resultant solution was then cooled, diluted by volume (25 mL) with 10% HCl, blended, and subjected to isotope analysis using a specifically created high-precision ICP-MS isotope analysis technique. Internal rock standards and

verified reference Pb isotopes were used to check precision and accuracy.

5 Analytical results

5.1 Mineral chemistry

According to the results of EMPA and LA-ICP-MS major and trace element mapping for pyrite, the Fe content of the Shihangli graphite deposit ranges from 44.3 to 46 wt%, with an average value of 45.57 wt%, and its S content ranges from 50.87 to 53.11 wt%, with an average value of 52.13 wt% (Table 2 and Fig. 3). The conventional value is equivalent to the atomic ratio of S/Fe, which generally ranges from 1.92 to 2.03.

Only 30 of the 39 elements studied were determined, and Ca, Sc, Ga, Rb, Cd, Tl, Ba, and In had element detection limits that had been exceeded. However, the Na, K, Sr, Ba, Mo, and W concentrations in certain pyrite grains were below the detection limit. Other elements, such as Ge, Se, Sn, Te, and W, only vary by one or two orders of magnitude, but the majority of element concentrations vary by three or four orders of magnitude (Fig. 2). The pyrite from the Shihangli graphite deposit has a high Co/Ni ratio (mean = 1.04 and ranges from 0.1 to 1.59), a high Ni (3–997 ppm), and a high Co concentration (presented in Table 2).

The Sb content in pyrite was similarly over the detection limit, with values ranging from 0.03 to 50.5 ppm (mean = 9.18 ppm; typical range, 0.53–12 ppm) (Table 2 and Fig. 3). Pyrite exhibits considerable As concentrations, ranging from 0.17 to 12,792 ppm (mean = 3120 ppm; typical range, 12.5–7800 ppm). Pyrite also contains significant quantities of the chalcophile elements Ag, Se, Pb, Se, Te, and Bi (Table 2 and Fig. 5). Au values in the Shihangli pyrite ranged from 0.006 to 1.05 ppm (mean = 0.20 ppm; typical range, 0.04–0.43 ppm), surpassing the detection limit (Table 2 and Fig. 3).

5.2 Lead isotopes

The lead isotope composition of pyrite from the Shihangli graphite deposit is shown in Table 3 and Fig. 6. The $^{206}\text{Pb}/^{204}\text{Pb}$ ratios of the samples range from 18.16 to 18.52, whereas the $^{207}\text{Pb}/^{204}\text{Pb}$ and $^{208}\text{Pb}/^{204}\text{Pb}$ ratios are 15.60 to 15.69 and 38.61 to 40.92, respectively. Similar Pb isotope compositions were observed in pyrite from the Shihangli graphite deposit, stibnite from the Xikuangshan Sb deposit, and Madiyi Formation bulk rock (Table 3 and Fig. 6).

Table 1 Sample list at the Shihangli coal-based graphite deposit

Sample	Location	Description
17SHL03	No. 3 quartz vein's at the No. 3 graphite ore footwall, Elevation = 200 m	Strongly silicified quartz sandstone, disseminated pyrite in the quartz vein width about 10–30 cm, occurrence of the quartz vein is $145^{\circ}/70^{\circ}$
17SHL04	No. 8 quartz vein's at the No. 3 graphite ore hanging wall, Elevation = 200 m	moderately silicified quartz sandstone, disseminated pyrite in the quartz vein width about 1–10 cm, occurrence of the quartz vein is $143^{\circ}/67^{\circ}$
17SHL05	No. 23 quartz vein's at the No. 3 graphite ore hanging wall, Elevation = 200 m	Strongly silicified siltstone, stellate distributed pyrite in the quartz vein width about 5–15 cm, occurrence of the quartz vein is $155^{\circ}/80^{\circ}$
17SHL06	No. 25 quartz vein's at the No. 3 graphite ore footwall, Elevation = 200 m	Silicified quartz sandstone, massive pyrite in the quartz vein width about 15–25 cm, occurrence of the quartz vein is $165^{\circ}/84^{\circ}$
17SHL07	No. 15 quartz vein's at the No. 3 graphite ore footwall, Elevation = 200 m	moderately silicified quartz sandstone, disseminated pyrite in the quartz vein width about 1–5 cm, occurrence of the quartz vein is $155^{\circ}/74^{\circ}$
17SHL08	No. 17 quartz vein's at the No. 3 graphite ore hanging wall, Elevation = 200 m	Strongly silicified siltstone, stellate distributed pyrite in the quartz vein width about 10–20 cm, occurrence of the quartz vein is $137^{\circ}/74^{\circ}$
17SHL09	No. 9 quartz vein's at the No. 3 graphite ore footwall, Elevation = 200 m	Silicified siltstone, disseminated pyrite in the quartz vein width about 0.3–1.5 cm, occurrence of the quartz vein is $146^{\circ}/71^{\circ}$

Table 2 EMPA and LA-ICP-MS major and trace elements in pyrite from Shihangli coal-based Graphite deposit

Sample	17SXL03-4	17SXL03-5	17SXL03-6	17SXL03-7	17SXL03-8	17SXL03-11	17SXL03-12	17SXL03-13	17SXL03-14	17SXL03-15	17SXL05-1	17SXL07-1	17SXL07-2
EMPA(wt%)													
S	52.790	51.530	51.650	51.460	52.270	52.250	52.630	51.700	51.960	51.440	50.870	52.770	51.920
Fe	45.800	44.310	45.300	45.710	45.840	45.700	45.580	45.220	44.990	45.620	45.330	45.650	45.410
Total	98.590	95.840	96.950	97.170	98.110	97.950	98.210	96.920	96.950	97.060	96.200	98.420	97.330
LA-ICP-MS(ppm)													
Mg	1.470	–	0.210	–	–	–	–	–	–	–	36.096	2.401	1.891
Al	37.700	13.768	0.318	1.030	4.860	2.562	5.997	2.211	14.147	0.987	88.043	10.564	1.391
Si	133.486	233.410	41.188	–	62.069	62.369	77.425	–	56.287	52.492	878.848	85.944	187.658
Ti	0.480	64.288	–	–	–	1.535	–	–	52.438	4.210	1.303	0.238	0.200
V	0.771	0.988	0.066	0.058	0.151	0.175	0.097	0.071	0.514	0.144	0.312	0.105	0.060
Cr	91.157	20.378	2.515	1.151	127.888	163.934	51.419	13.458	29.328	32.288	7.385	50.995	0.579
Mn	0.533	0.534	0.386	0.342	0.465	0.393	0.321	0.345	0.362	0.310	2.940	4.276	18.767
Co	191.116	562.012	17.104	1.012	1.440	173.006	31.505	7.795	7.200	27.006	1.606	12.563	150.436
Ni	346.341	997.507	12.503	3.012	6.768	215.620	53.593	26.530	61.314	5.236	655.653	17.265	50.667
Cu	5.822	5.038	4.203	4.783	2.292	4.089	5.905	9.258	4.483	2.064	94.897	0.718	8.294
Zn	6.271	1.553	0.604	0.468	1.892	1.811	0.820	0.687	1.719	0.810	5.515	0.987	0.875
Ge	1.642	1.411	1.802	1.796	1.473	1.610	1.530	1.394	1.434	1.438	2.425	1.264	1.186
As	9240	3056	12.792	8190	977	11.264	5251	9805	7722	8033	31.54	76.28	15.15
Se	56.513	24.828	81.380	72.581	98.253	68.201	128.902	129.395	72.887	58.148	7.229	2.970	6.235
Y	0.286	0.263	0.010	0.024	0.101	0.106	0.008	0.020	0.303	0.073	5.441	0.035	0.383
Mo	0.043	–	–	–	0.025	0.079	–	–	0.018	0.017	0.202	0.029	0.172
Ag	0.036	0.285	0.018	0.621	3.362	0.007	0.006	0.062	0.024	0.013	0.586	0.029	0.214
Sn	0.093	0.338	0.048	–	0.107	–	–	–	0.247	–	0.281	–	0.283
Sb	0.430	4.164	0.567	9.439	6.762	0.032	0.104	0.673	0.423	0.109	19.707	1.464	9.487
Te	3.282	0.882	5.085	1.350	0.769	1.041	4.803	9.466	4.573	4.832	0.199	0.523	1.232
W	0.010	–	–	–	0.009	–	–	–	0.078	0.022	0.266	–	–
Au	0.296	0.257	1.051	0.472	0.006	0.858	0.341	0.740	0.389	0.206	0.038	–	–
Bi	0.046	0.244	0.094	1.707	7.979	0.008	0.013	0.209	0.072	0.018	6.554	1.015	18.366
Pb	1.653	16.972	0.870	68.549	545.004	0.061	0.089	1.630	0.591	0.222	151.275	8.318	112.842
Th	0.320	0.037	–	0.003	0.053	0.014	0.007	0.004	0.190	0.041	0.529	–	0.004
U	0.044	0.016	0.003	0.006	0.106	0.044	0.068	0.003	0.043	0.017	0.110	0.003	0.002
Co/Ni	0.552	0.563	1.368	0.336	0.213	0.802	0.588	0.294	0.117	5.158	0.002	0.728	2.969
Zn/Ni	0.018	0.002	0.048	0.155	0.280	0.008	0.015	0.026	0.028	0.155	0.008	0.057	0.017
Cu/Ni	0.017	0.005	0.336	1.588	0.339	0.019	0.110	0.349	0.073	0.394	0.145	0.042	0.164
S/Fe	2.008	2.026	1.986	1.961	1.986	1.991	2.011	1.991	2.012	1.964	1.955	2.013	1.991

Sample	17SXL07-3	17SXL07-4	17SXL07-5	17SXL07-7	17SXL07-8	17SXL07-9	17SXL07-10	17SXL07-11	17SXL07-4	17SXL09-6	17SXL09-10	17SXL09-11	17SXL09-12
EMPA(wt%)													
S	51.870	52.610	52.300	52.010	52.920	53.110	52.380	52.060	51.970	52.530	52.080	52.090	52.090
Fe	45.920	45.990	45.780	45.660	45.980	45.920	45.970	45.740	45.560	45.750	44.650	45.940	45.610
Total	97.790	98.600	98.080	97.670	98.900	99.030	98.350	97.800	97.530	98.280	96.730	98.030	97.700
LA-ICP-MS(ppm)													
Mg	0.553	0.212	-	9.234	3.459	0.248	2.991	6.805	86.227	1.717	12.725	5.249	109.580
Al	0.530	2.355	0.699	64.403	2.944	3.350	13.280	36.793	186.732	15.367	33.413	41.481	187.096
Si	80.917	43.432	623.758	413.164	64.101	65.389	226.007	165.848	3724.589	61.067	433.605	744.153	954.654
Ti	0.220	0.466	0.290	0.234	0.614	0.385	0.442	0.847	50.717	0.161	885.849	0.561	119.487
V	0.053	0.051	0.039	0.137	0.054	0.169	0.238	0.474	2.206	0.074	5.819	0.905	1.382
Cr	0.279	2.041	0.732	11.533	3.814	78.416	59.108	14.396	104.570	66.691	298.553	348.384	111.270
Mn	1.580	0.378	0.264	30.197	28.449	1.145	44.349	294.164	5.857	2.473	1.251	0.666	6.212
Co	118.114	0.695	42.560	147.944	25.654	0.357	0.265	0.479	3.911	54.230	56.270	47.048	28.879
Ni	37.570	3.144	16.423	29.988	13.341	688.136	376.266	141.823	20.803	285.039	552.099	569.752	374.695
Cu	10.491	4.910	23.346	6.230	0.500	1.037	5.917	2.034	17.810	4.343	5.876	18.375	13.879
Zn	0.803	0.681	0.826	0.769	0.856	1.893	1.691	1.901	4.535	1.380	5.689	4.933	5.351
Ge	1.487	1.220	1.287	1.266	1.467	1.136	1.429	1.076	1.956	1.418	1.500	1.265	1.257
As	12.908	3.214	11.450	0.172	0.793	1.370	19.988	0.372	1893	67.204	1172	840.049	644.185
Se	7.858	1.723	8.232	7.215	4.324	14.612	9.953	2.418	4.659	7.292	8.871	8.224	6.272
Y	0.002	4.003	-	0.748	0.138	0.036	0.058	0.142	0.409	0.064	1.940	0.070	1.621
Mo	0.159	0.130	0.197	0.380	0.258	0.025	0.501	0.236	0.073	0.526	0.070	0.568	0.021
Ag	0.239	0.132	0.491	0.277	0.070	0.122	1.646	0.777	0.451	0.074	0.105	0.250	0.194
Sn	0.399	0.217	0.876	0.304	0.028	0.736	0.213	1.505	0.073	-	0.436	0.209	0.351
Sb	16.883	9.207	50.487	9.659	0.662	1.372	0.787	0.198	20.023	4.007	10.306	21.275	40.343
Te	1.445	-	0.575	1.666	0.125	-	-	0.134	0.708	3.347	4.120	2.747	2.348
W	-	-	-	-	-	0.034	0.015	-	0.035	-	0.488	0.013	0.031
Au	0.008	-	-	-	-	-	-	-	0.051	0.020	0.043	0.123	0.316
Bi	19.450	5.418	29.293	16.970	1.930	0.058	0.600	0.730	4.187	3.642	2.827	5.214	3.915
Pb	170.246	74.874	445.648	113.480	6.955	4.265	10.504	2.908	152.539	24.360	51.894	153.518	239.101
Th	-	0.024	0.003	0.003	-	-	0.010	0.017	0.030	0.012	0.406	0.057	0.096
U	-	0.061	-	0.014	0.006	0.018	0.023	0.014	0.082	0.016	1.013	0.103	0.141
Co/Ni	3.144	0.221	2.592	4.933	1.923	0.001	0.001	0.003	0.188	0.190	0.102	0.083	0.077
Zn/Ni	0.021	0.216	0.050	0.026	0.064	0.003	0.004	0.013	0.218	0.005	0.010	0.009	0.014
Cu/Ni	0.279	1.562	1.422	0.208	0.037	0.002	0.016	0.014	0.856	0.015	0.011	0.032	0.037
S/Fe	1.967	1.992	1.990	1.984	2.005	2.014	1.985	1.982	1.987	2.000	2.032	1.975	1.989

“-” means under the detection limit

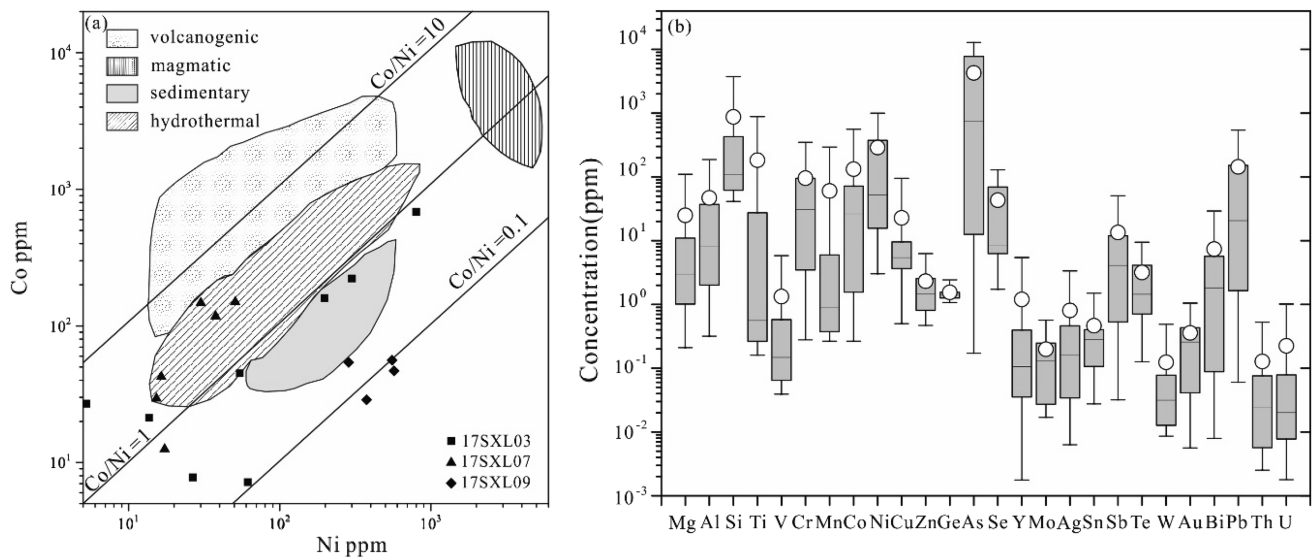


Fig. 5 **a** Co–Ni diagram and **b** box and whisker plot for pyrite from quartz veins in the Shihangli graphite deposit (**a** is based on Bajwah et al. 1987, Brill 1989, and Xu 1998)

Table 3 Lead isotope systematics of pyrite from the Central Hunan, South China

Sample	$^{206}\text{Pb}/^{204}\text{Pb}$	$^{207}\text{Pb}/^{204}\text{Pb}$	$^{208}\text{Pb}/^{204}\text{Pb}$	$^{206}\text{Pb}/^{207}\text{Pb}$	mineral	references
17SHL04	18.52	15.69	38.92	1.1804	pyrite	this paper
17SHL05	18.31	15.74	38.91	1.1633		
17SHL07	18.31	15.67	38.68	1.1685		
17SHL08	18.16	15.6	38.61	1.1641		
S939	18.423	15.788	38.865	1.1669	Stibnite of Xikuangshan Sb deposit	(Hu 1995)
S937	18.139	15.573	38.32	1.1648		
S9326	18.326	15.613	38.471	1.1738		
N932	18.272	15.674	38.538	1.1658		
BW-1	17.528	15.465	39.028	1.1334	Bulk of Wuqianxi formation	(Liu and Zhu 1994)
BW-10	17.507	15.46	37.897	1.1324		
BW-18	18.318	15.524	39.163	1.18		
BW-12	18.338	15.526	39.455	1.1811		
BM-1	18.297	15.705	38.854	1.165	bulk of Madiyi Formation	
BM-5	17.647	15.572	38.354	1.1333		
BM-10	18.396	15.657	38.759	1.1749		
BM-12	17.821	15.555	38.509	1.1457		
BM-20	18.266	15.591	39.971	1.1716		
BM-21	17.733	15.553	38.542	1.1402		
BM-22	18.223	15.632	39.753	1.1657		
BM-3	17.768	15.572	38.701	1.141		
L-2	18.832	15.586	39.294	1.2083	bulk of Lengjiayi group	
L-7	19.034	15.59	39.858	1.2209		
L-60	20.525	15.788	41.792	1.3		
L-11-1	19.122	15.642	40.057	1.2225		

5.3 Re–Os isotopes

In pyrite, the $^{187}\text{Re}/^{188}\text{Os}$ and $^{187}\text{Os}/^{188}\text{Os}$ ratios were 3027–5754 and 8.09–13.34, respectively, whereas the total Re and Os abundances were 7.37–15.56 and 0.019–0.046 ppb, respectively (Table 4). The samples showed a positive relationship between $^{187}\text{Re}/^{188}\text{Os}$ and $^{187}\text{Os}/^{188}\text{Os}$ (Fig. 7a). The Re–Os model pyrite ages of Shihangli ranged from 137 to 146 Ma (Table 4), with a weighted mean age of 143.5 Ma (MSWD = 1.4). (Fig. 7b). The pyrite yielded an individual Re–Os isochron age of 127.6 ± 3.8 Ma (MSWD = 1.4, beginning $^{187}\text{Os}/^{188}\text{Os}$ ratio = 1.03 ± 0.24) (Fig. 7a).

After the common Os was modified, the Re–Os model age of Shihangli pyrite ranged from 125.3 to 128.1 Ma (Table 4). The age of the Re–Os isochron (127.6 ± 3.8 Ma) was quite close to this figure (Fig. 6a). Shihangli pyrite had an Os(t) range of 603.7–792.5.

6 Discussion

6.1 Mineralogenesis of pyrite from the Shihangli graphite deposit

The mineralogy and electron microprobe investigation of pyrite from graphite quartz veins in Shihangli revealed that pyrite is predominantly found in hydrothermal quartz veins (Figs. 3a, b). According to in situ LA-ICP-MS trace element tests, the point Sb concentration of pyrite ranged from 0.03 to 50.5 ppm (mean = 9.2 ppm, typically between 0.5 and 11.2 ppm) (Table 2 and Fig. 5b). The Shihangli pyrite was high in As, with average values ranging from 17.4 to 7800 ppm. Based on research using the LA-ICP-MS trace

element mapping technique, the pyrite from the Shihangli graphite mine is usually rich in As, Au, Pb, Sb, and other ore-forming elements (Table 2 and Fig. 5b). The Co–Ni diagram shows that most of the pyrite in sample 17SHL07, as well as the typical Co/Ni ratios of 0.1–1.5 for pyrite in the Shihangli deposit, is hydrothermal in origin (Fig. 5a and Table 2). The extremely low Se content of this pyrite (ranging from 1.7 to 14.6 ppm), which is comparable to the value of sample 17SHL09 (4.9–8.9 ppm) (Table 2), indicates a hydrothermal origin. The Co–Ni diagram (Fig. 5a) shows that some of the pyrites in sample 17SHL03 are of sedimentary origin and may have formed due to a water/rock interaction in coal measure layers. This pyrite is also notable for having a higher Se concentration (between 24.8 and 129 ppm) (Table 2). The pyrite of the Shihangli graphite deposit appears to have formed on a vast scale from an Sb–Au–As rich ore-forming fluid in Central Hunan, South China, when coupled with local metallogenic features.

6.2 Os and Pb isotopes of pyrite trace the origin of ore-forming fluids in Sb–Au mineralization

The initial $^{187}\text{Os}/^{188}\text{Os}$ and Os values can be used to establish the origin of Re–Os and the proportion of crustal components that enter protomagma (Ackerman et al. 2013; Foster et al. 1996; Han et al. 2007; Jiang 2000). The compositions of pyrite Pb isotopes reveal information on the history of metallogenic fluid in hydrothermal deposits and the origin of the minerals found there. As a result, the Re–Os, and Pb isotope compositions in hydrothermal pyrite may be used to determine the origin of Sb and Au mineralization in Central Hunan.

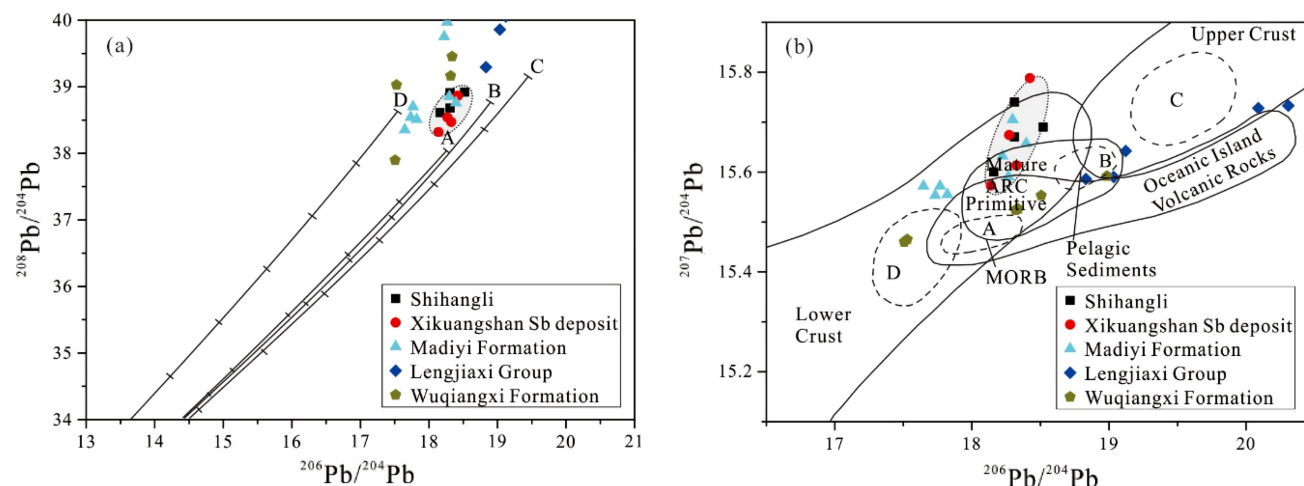


Fig. 6 **a** Pb isotope sources in pyrite, stibnite, and Neoproterozoic epimetamorphic rock in Central Hunan, southern China. **b** Tectonic model of the Pb isotope of pyrite from the Shihangli graphite deposit (after Zartman and Doe 1981)

Table 4 Re-Os isotope systematics of pyrite from the coal-based coal-based graphite deposit

Sample Number	Weight g	Re ng/g		Common Os ng/g		$^{187}\text{Re}/^{188}\text{Os}$		$^{187}\text{Os}/^{188}\text{Os}$		Model Age(Ma) ^b	Model Age(Ma) ^c	$\gamma\text{Os}(t)$
		Content	Uncertainty	Content	Uncertainty	Content	Uncertainty	Content	Uncertainty			
17SHL03	1.1	15.556	0.068	0.046179	0.000214	3307.4	21.1	8.0880	0.0597	146.6	127.6	745.1
17SHL05	1.2	8.998	0.051	0.024510	0.000034	3905.0	23.0	9.3904	0.0239	144.2	128.1	771.8
17SHL06	1.5	7.367	0.033	0.022952	0.000034	3026.6	14.2	7.4687	0.0219	147.9	127.2	726.7
17SHL07	1.0	7.619	0.050	0.018545	0.000052	4813.1	34.5	11.1063	0.0642	138.3	125.3	603.7
17SHL09	0.8	14.394	0.103	0.032821	0.000051	5754.4	42.3	13.3429	0.0349	139.0	128.1	792.5

a Initial $^{187}\text{Os}/^{188}\text{Os}$ ratio derived from isochron (Fig. 5a)

b Model age calculated without removing common Os

c Model age calculated after removing common Os using initial $^{187}\text{Os}/^{188}\text{Os}$ ratio of 1.03 ± 0.24

d $\gamma\text{Os}(t) = 100 \times [({}^{187}\text{Os}/^{188}\text{Os})_t / ({}^{187}\text{Os}/^{188}\text{Os})_{\text{chondrite}(t)} - 1]$, $({}^{187}\text{Os}/^{188}\text{Os})_{\text{detection}} = ({}^{187}\text{Re}/^{188}\text{Os}) \times (e^{t-1})$

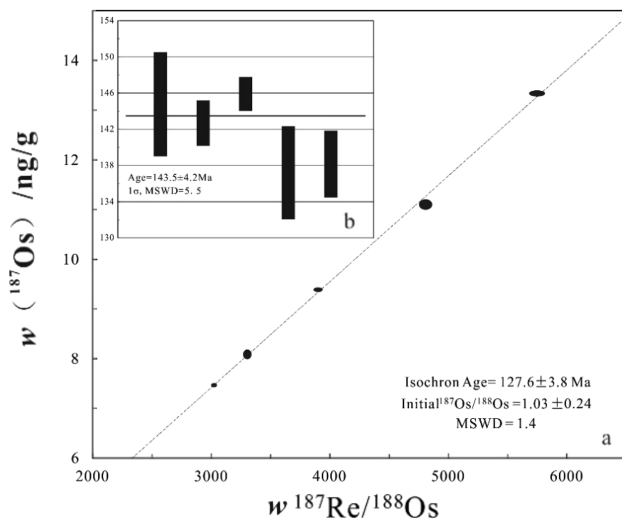


Fig. 7 **a** Re–Os isochron age and **b** weighted average age of pyrite from the coal-based graphite deposit in Central Hunan, southern China (plotted in Isoplot 4.15)

The initial ($^{187}\text{Os}/^{188}\text{Os}$) value calculated from the pyrite Re–Os isochron is 1.03 ± 0.24 (Fig. 7a), which is much greater than the value of the Cu–Ni sulfide deposit and any anticipated mantle value but much lower than the typical value found in the continental crust (3.63). Hydrothermal pyrite from Shihangli is radioactively enriched in $^{187}\text{Os}/^{188}\text{Os}$ (7.47–13.3). Additionally, it is generally compatible with the initial ratio of 1.04 ± 0.16 (Arne et al. 2001). In Shihangli, the $\gamma_{\text{Os}}(t)$ values of the pyrite vary from 572 to 755 (Table 4). This is quite similar to the values reported in the Sudbury Proterozoic Metasedimentary Rocks (844–1054) (Palmer and Turekian 1986), but considerably higher than the average value of what is found in continental crust, which is 3.63 (Walker et al. 1991). Consequently, the initial ($^{187}\text{Os}/^{188}\text{Os}$) and Os(t) observations suggest that the Re–Os of hydrothermal pyrite from the Shihangli graphite deposit may have come from Neoproterozoic basement metamorphic rocks in Central Hunan. This is consistent with previous findings demonstrating the origin of ore-forming elements (Sb, Au, and As) in basement metamorphic rocks (Ma et al. 2002, 2003). It was also discovered that ore-forming elements (Sb, Au, and As) were transferred from the basement metamorphic rocks of Central Hunan into the caprock by hydrothermal extraction (Ma et al. 2003; Peng and Frei 2004; Peng and Hu 2001; Peng et al. 2002).

The Pb isotope compositions of pyrite from the Shihangli graphite deposit and bulk rock from the Wuqiangxi Formation and Lengjiayi Group are markedly different (Table 3 and Fig. 6). However, the Shihangli graphite deposit pyrite has a Pb isotope composition similar to the Madiyi Formation bulk rock and stibnite from the Xikuangshan Sb deposit (Table 3 and Fig. 6). Therefore,

indicating sulfides of the two deposits probably originated from the Neoproterozoic Madiyi Formation. This conclusion is supported by the fact that the ore-forming elements of the pyrite from the Shihangli graphite deposit and the Sb deposit of the Central Hunan origin from the Madiyi Formation are revealed by Pb isotope ratios of sulfides in the Woxi deposit, Sr and Os isotopic signatures of the Banxi Sb deposit, H–O–S–Pb isotope, and rare earth element characteristics of the Xikuangshan, Dong’an Sb deposit (Li et al. 2019, 2020b, 2022; Zhou et al. 2023a; Liu et al. 2023).

According to the Re–Os, Sr, S, and Pb isotopic compositions of sulfides in the Sb deposit in Central Hunan, the Madiyi Formation, particularly, may have been the major source of ore-forming elements such as Sb and Au in the Upper Paleozoic strata.

6.3 Re–Os isotopic age of pyrite implication to the timing of large-scale fluid transportation and coal-generated graphite mineralization in Central Hunan

Pyrite mineralization in Shihangli has a Re–Os isochron age of 127.6 ± 3.8 Ma (Table 4 and Fig. 7a). The Re–Os age of pyrite is similar to previous Sm–Nd dating of hydrothermal calcite (124 Ma) (Peng et al. 2003a) as well as in situ U–Pb dating of calcite (115.3 ± 1.5 Ma) from the Weizhai Sb Deposit (Luo et al. 2020). The Banxi Sb–(Au–W) deposit, like the Xikuangshan Sb deposit, is a typical low-temperature mineralization Sb deposit. This deposit is located in the notable Central Hunan Sb belt in South China, where Neoproterozoic epimetamorphic clastic sedimentary rocks contain quartz vein-type Sb-only mineralization (Li et al. 2019). Re–Os pyrite from the Shihangli deposit has excellent agreement with the (U–Th)/He age of zircon (123.8 ± 3.8 Ma), the Rb–Sr age of sulfides (129.4 ± 2.4 Ma), and the Sm–Nd age of sulfides (130.4 ± 1.9 Ma) from the Banxi Sb deposit (Li et al. 2018a, 2020a), which are thought to date the low-temperature mineralization stage in Central Hunan. This demonstrates that the age range of low-temperature hydrothermal mineralization in Central Hunan is constant. Additionally, this suggests that the Yanshanian hydrothermal activity in Central Hunan has widespread basin-scale characteristics rather than being isolated within the metallic mineral deposit.

Based on the Re–Os dating of quartz vein pyrite, the Shihangli graphite deposit experienced significant siliceous alteration in the Yanshanian. The Yanshanian may have witnessed the transition of coal into graphite in the Lower Carboniferous Ceshui Formation in Central Hunan. Previous research indicates that regional magmatic thermal change (graphitization) occurred in the coal-bearing strata

of the Ceshui Formation throughout the Late Triassic and Middle Jurassic (Bi et al. 1996). The Re–Os isotope age of pyrite limits the magmatic thermal history of the area to the early Cretaceous. During the early Cretaceous, there appears to have been extensive coal metamorphism and hydrothermal alteration in Central Hunan, coinciding with the regional Sb and Au metallogenic events.

The Re–Os isochron dating of hydrothermal pyrite from the Shihangli graphite deposit demonstrates that significant fluid movement and basin-wide mineralization occurred during the Yanshanian in Central Hunan. The associated hydrothermal events should have occurred after the coal measures were deposited (in the Carboniferous–Permian). However, this age range (125.3–128.1 Ma) does not rule out the possibility that the Ceshui Formation coal measures underwent their initial thermal evolution in the Early Carboniferous and Middle Triassic (Bi et al. 1996). The Re–Os isochron age of pyrite (Fig. 7a), which coincides with current geological data, dates it to the Yanshanian era. The LA-ICP-MS data also demonstrate that pyrite associated with hydrothermal quartz veins has high As, Au, Pb, Sb, and other ore-forming element concentrations (Table 2).

Consequently, a fluid with a comparable composition to an ore-forming fluid was most likely the source of the quartz vein in the Shihangli graphite deposit. The coal measures in Central Hunan are widely scattered and often exposed to thermal metamorphism, wall rock alteration, and quartz/calcite vein intercalation, implying that hydrothermal superimposition should be a large-scale regional fluid event. In several coal samples, hydrothermal fluid rich in Sb, As, Au, Co, Bi, Pb, and Si may have undergone metamorphism (graphitization) and significant silicification alteration (Bi et al. 1996, 1997; He et al. 2002). As a result of the enrichment and mineralization of scattered elements on a regional scale, small Sb–Au deposits and even exceptionally large Sb deposits were formed due to the migration and expansion of large-scale ore-forming fluids. This research backs up the synchronicity of the Yanshanian ore-forming fluid and the possibility of large-scale fluid movement and coal-generated graphite mineralization in Central Hunan, South China.

7 Conclusions

- (1) The Shihangli deposit features Co/Ni ratios greater than 1, with concentrations ranging from 0.1 to 1.5, and the pyrite has a high As level (0.17–12792 ppm, concentrated in 17.4–7800 ppm) and very low Se content (1.7–129.4 ppm). This indicates that the primary pyrite in the Shihangli graphite deposit is

hydrothermal pyrite, which is typically rich in ore-forming elements such as As, Au, Pb, and Sb.

- (2) The Pb isotope composition of the hydrothermal pyrite from the Shihangli deposit is comparable to that of the bulk rock of the Madiyi Formation and the stibnite from the Xikuangshan Sb deposit. This pyrite has a high radiogenic $^{187}\text{Os}/^{188}\text{Os}$ concentration ranging from 7.5 to 13.3, with an initial $^{187}\text{Os}/^{188}\text{Os}$ value of 1.030.24. According to the Re–Os, Sr, S, and Pb isotopic compositions of sulfides in the Sb deposit in Central Hunan, the Madiyi Formation, particularly, may have been the primary source of ore-forming elements such as Sb and Au in the upper Paleozoic strata.
- (3) Pyrite from the Shihangli graphite deposit was dated using Re–Os (127.6 ± 3.8 Ma), and it is the age of large-scale hydrothermal alteration and coal-generated graphite deposits in Central Hunan.

Acknowledgements This research was funded by the National Key Research and Development Program of China (2016YFC0600207 and 2014CB440904), the National Natural Science Foundation of China (Nos. 42062006 and 41962007), and the Integrated Exploration Project of China Geological Survey (No. 12120114034501). This paper is largely based on data obtained for a Ph.D. project at the Nanjing University, China. We would like to thank the two reviewers and editors very much for their constructive comments.

Author contribution YZ conceived of the presented idea and developed the theoretical formalism after wrote the manuscript. XPL, GL, FJZ, XTZ, and YL helped complete sample processing and testing. DSM, J-FG, and JP contributed to the final version of the manuscript.

Funding This research was funded by the National Key Research and Development Program of China (2016YFC0600207 and 2014CB440904), National Natural Science Foundation of China (Nos. 42062006 and 41962007), and the Integrated Exploration Project of China Geological Survey (No. 12120114034501). This paper is largely based on data obtained for a PhD project at the Nanjing University, China. We would like to thank the two reviewers and editors very much for their constructive comments.

Data availability The results from our study is our original unpublished work and it has not been submitted to any other journal for reviews.

Code availability There are no software application or custom code.

Declarations

Conflict of interest On behalf of all authors, the corresponding author states that there is no conflict of interest. Jian-Feng Gao is editorial board member of *Acta Geochimica*. He was not involved in the journal's review of, or decisions related to, this manuscript. The authors have no other competing interests to disclose.

Ethics approval This manuscript we wish to be considered for publication in "*ACTA Geochimica*". No conflict of interest exists in the submission of this manuscript, and manuscript is approved by all

authors for publication. I would like to declare on behalf of my co-authors that the work described was original research that has not been published previously, and not under consideration for publication elsewhere, in whole or in part. All the authors listed have approved the manuscript that is enclosed.

Consent to participation We agree to participate in the arrangement of manuscript submission by the editorial department of the journal.

Consent for publication We agree to publish this manuscript.

References

- Ackerman L, Pašava J, Erban V (2013) Re–Os geochemistry and geochronology of the Ransko gabbro–peridotite massif Bohemian Massif. *Miner Depos* 48(7):799–804
- Akiska S, Demirela G, Sayili S (2013) Geology, mineralogy and the Pb, S isotope study of the Kalkım Pb–Zn±Cu deposits, Biga Peninsula, NW Turkey. *J Geosci* 379–396
- An JH, Tang FP, Li J (2016) Metallogenic rules and resource potential of the graphite deposit in Hunan province. *J Geol* 40(3):433–437
- Arne D, Bierlin F, Morgan J, Stein H (2001) Re–Os dating of sulfides associated with gold mineralization in central Victoria. *Aust Econ Geol* 96(6):1455–1459
- Bajwah ZU, Seccombe PK, Offler R (1987) Trace element distribution Co: Ni ratios and genesis of the big cadia iron-copper deposit, new south wales, australia. *Miner Depos* 22(4):292–300
- Bi H (1998) The characteristics of X-Ray diffraction for coal of Ceshui formation in Lianyuan coal Basin. *J Mineral Petrol* 18(3):8–11 (in Chinese with English abstract)
- Bi H, Peng GL, Yang MH (1996) The thermal history and hydrocarbon-generating characteristics of Ceshui and Longtan coal series in Lianyuan, Hunan Province. *J East China Geol Instit* 19(2):157–161 (in Chinese with English abstract)
- Bi H, Peng GL, Zhong JH (1997) The regional magmatic thermal metamorphism of the Ceshui formation coal in Lianyuan Coal Basin. *J China Coal Soc* 22(4):349–354 (in Chinese with English abstract)
- Brill BA (1989) Trace-element contents and partitioning of elements in ore minerals from the CSA Cu–Pb–Zn deposit. *Aust Can Mineral* 27(7):263–274
- Chen WF, Chen PR, Huang HY, Ding X, Sun T (2007) Chronological and geochemical studies of granite and enclave in Baimashan pluton, Hunan South China. *Sci China-Earth Sci* 50(11):1606–1627 (in Chinese with English abstract)
- Dai JF, Xu DR, Chi GX, Li ZH, Deng T, Zhang J, Li B (2022) Origin of the Woxi orogenic Au–Sb–W deposit in the west Jiangnan Orogen of South China: constraints from apatite and wolframite U–Pb dating and pyrite in-situ S–Pb isotopic signatures. *Ore Geol Rev* 150:105134
- Deng XH, Wang JB, Pirajno F, Wang YW, Li YC, Li C, Zhou LM, Chen YJ (2016) Re–Os dating of chalcopyrite from selected mineral deposits in the Kalatag district in the eastern Tianshan Orogen China. *Ore Geol Rev* 77:72–81
- Duan SG, Jiang ZS, Zhang ZH, Li FM, Ren YQ (2017) Re–Os isotopic analysis of pyrrhotite from Tianyu Cu–Ni sulfide deposit in Eastern Tianshan Mountains, Xinjiang: constraints on sources of ore-forming materials. *Mineral Depos* 36(01):25–37 (in Chinese with English abstract)
- Fan DL, Zhang T, Ye J (2004) The Xikuangshan Sb deposit hosted by the upper Devonian black shale series, Hunan. *China Ore Geol Rev* 24(1–2):121–133
- Foster JG, Lambert DD, Frick LR, Maas R (1996) Re–Os isotopic evidence for genesis of Archaean nickel ores from uncontaminated komatiites. *Nature* 382(6593):703–706
- Fu SL, Hu RZ, Chen YW, Luo JC (2016) Chronology of the longshan Au–Sb deposit in central hunan province: constraints from pyrite Re–Os and zircon U–Th/He isotopic dating. *Acta Petrol Sinica* 32(11):3507–3517 (in Chinese with English abstract)
- Fu SL, Hu RZ, Batt GE, Danišik M, Evans NJ, Mi XF (2020a) Zircon (U–Th)/He thermochronometric constraints on the mineralization of the giant Xikuangshan Sb deposit in central Hunan South China. *Miner Depos* 55(5):901–912
- Fu SL, Lan Q, Yan J (2020b) Trace element chemistry of hydrothermal quartz and its genetic significance: a case study from the Xikuangshan and Woxi giant Sb deposits in southern China. *Ore Geol Rev* 126:103732
- Han CM, Xiao WJ, Zhao GC, Qu WJ, Du AD (2007) Re–Os dating of the Kalatongke Cu–Ni deposit, Altay Shan, NW China, and resulting geodynamic implications. *Ore Geol Rev* 32(1):452–468
- He MY, Lou YE, Wang P (2002) Relationship between silicification and stibnite mineralization in Xikuangshan antimony deposit. *Hunan Prov Mineral Depos* 21(S1):384–387 (in Chinese with English abstract)
- He HS (2008) The characters of cal-bearing formation and coalfield prediction of Ceshui formation of Carboniferous in Middle Hunan [Master]. Changsha: Central South University, 1–59 (in Chinese with English abstract)
- Hnatyshin D, Creaser RA, Wilkinson JJ, Gleeson SA (2015) Re–Os dating of pyrite confirms an early diagenetic onset and extended duration of mineralization in the Irish Zn–Pb ore field. *Geology* 43(2):143–146. <https://doi.org/10.1130/G36296.1>
- Hu RZ, Chen WT, Xu DR, Zhou MF (2017) Reviews and new metallogenic models of mineral deposits in South China: an introduction. *J Asian Earth Sci* 137:1–8
- Hu XW (1995) The geological setting and genesis of Xikuangshan super-giant antimony deposits, Hunan, China. Beijing: Chinese Acad Geol Sci 1–173 (in Chinese with English abstract)
- Huang GX, He YD, Deng T, Dai B (1985) Survey data of local coal mines in Hunan Province: coal mine of Loudi city, Hunan province (III). *Coal Ind Dep Hunan Prov Changsha*, 1–359 (in Chinese)
- Jemmali N, Souissi F, Carranza EJM, Bouabdellah M (2013a) Lead and sulfur isotope constraints on the genesis of the polymetallic mineralization at Oued Maden, Jebel Hallouf and Fedj Hassene carbonate-hosted Pb–Zn (As–Cu–Hg–Sb) deposits, Northern Tunisia. *J Geochem Explor* 132:6–14
- Jemmali N, Souissi F, Carranza EJM, Vennemann TW (2013b) Sulfur and lead isotopes of Guern Halfaya and Bou Grine deposits (Domes zone, northern Tunisia): implications for sources of metals and timing of mineralization. *Ore Geol Rev* 54:17–28
- Jiang SY (2000) Controls on the mobility of high field strength elements (HFSE), U, and Th in an ancient submarine hydrothermal system of the proterozoic Sullivan Pb–Zn–Ag deposit, British Columbia. *Canada Geochem J GJ* 34(5):341–348
- Jiang SY, Yang JH, Zhao KD, Yu JM (2000) Re–Os isotope tracer and dating methods in ore deposits research. *J Nanjing Univ Natl Sci* 36(06):669–677 (in Chinese with English abstract)
- Kang RH (2002) Analysis of exploration perspectives of gold-antimony deposits in Baimashan-Longshan ew-striking structural zone, Hunan province. *Geol Mineral Resour South China* 1:57–61 (in Chinese with English abstract)
- Kuang WL (2000) Research on the metallogenic model of Xikuangshan Superlarge antimony deposit. *World Geol* 19(1):26–30 (in Chinese with English abstract)
- Laznicka P (1999) Quantitative relationships among giant deposits of metals. *Econ Geol* 94(4):455–473

- Li XH, Li WX, Li ZX, Lo CH, Wang J, Ye MF, Yang YH (2009) Amalgamation between the Yangtze and Cathaysia Blocks in South China: Constraints from SHRIMP U–Pb zircon ages, geochemistry and Nd–Hf isotopes of the Shuangxiwu volcanic rocks. *Precambr Res* 174(1):117–128
- Li HT, Cao DY, Wang LJ, Guo AJ, Li YF, Xu H (2013) Characteristics and evolution of coal-controlled structures on the east slope of the Xuefengshan domain in central Hunan province. *Geotecton Metallog* 37(4):611–621 (in Chinese with English abstract)
- Li J, Jiang XY, Xu JF, Zhong LF, Wang XC, Wang GQ, Zhao PP (2014) Determination of platinum-group elements and Re–Os isotopes using ID-ICP-MS and N-TIMS from a single digestion after two-stage column separation. *Geostand Geoanal Res* 38(1):37–50 (in Chinese with English abstract)
- Li J, Wang XC, Xu JF, Xu YG, Tang GJ, Wang Q (2015a) Disequilibrium-induced initial Os isotopic heterogeneity in gram aliquots of single basaltic rock powders: Implications for dating and source tracing. *Chem Geol* 406:10–17
- Li J, Zhao PP, Liu JG, Wang XC, Yang AY, Wang GQ, Xu JF (2015b) Reassessment of hydrofluoric acid desilicification in the carius tube digestion technique for Re–Os isotopic determination in geological samples. *Geostand Geoanal Res* 39(1):17–30 (in Chinese with English abstract)
- Li HT, Li JZ, Li Y, Liang H, Li LH (2017) Coal seam deformation and metamorphism characteristics in central Hunan. *J Xian Univ Ence Technol* 37(6):886–891 (in Chinese with English abstract)
- Li H, Wu Q-H, Evans NJ, Zhou Z-K, Kong H, Xi X-S, Lin Z-W (2018a) Geochemistry and geochronology of the Banxi Sb deposit: Implications for fluid origin and the evolution of Sb mineralization in central-western Hunan. *South China Gondwana Res* 55:112–134
- Li X-Y, Gao J-F, Zhang R-Q, Lu J-J, Chen W-H, Wu J-W (2018b) Origin of the Muguayuan veinlet-disseminated tungsten deposit, South China: constraints from in-situ trace element analyses of scheelite. *Ore Geol Rev* 99:180–194
- Li H, Kong H, Zhou Z-K, Tindell T, Tang Y-Q, Wu Q-H, Xi X-S (2019) Genesis of the Banxi Sb deposit, South China: constraints from wall-rock geochemistry, fluid inclusion microthermometry, Rb–Sr geochronology, and H–O–S isotopes. *Ore Geol Rev* 115:103162
- Li H, Danišić M, Zhou Z-K, Jiang W-C, Wu J-H (2020a) Integrated U–Pb, Lu–Hf and (U–Th)/He analysis of zircon from the Banxi Sb deposit and its implications for the low-temperature mineralization in South China. *Geosci Front* 11(4):1323–1335
- Li H, Kong H, Guo B-Y, Soh TL, Zhang Q, Wu Q-H, Xi X-S (2020b) Fluid inclusion, H–O–S isotope and rare earth element constraints on the mineralization of the Dong’an Sb deposit South China. *Ore Geol Rev* 126:103759
- Li H, Zhu D-P, Shen L-W, Algeo TJ, Elatikpo SM (2022) A general ore formation model for metasediment-hosted Sb–(Au–W) mineralization of the Woxi and Banxi deposits in South China. *Chem Geol* 607:121020
- Liu HC, Zhu BQ (1994) Geochronology study of Banxi group and Lengjiaxi group from Western Hunan. *Chin Sci Bull* 39(2):148–150 (in Chinese with English abstract)
- Liu YS, Hu ZC, Gao S, Günther D, Xu J, Gao CG, Chen HH (2008) In situ analysis of major and trace elements of anhydrous minerals by LA-ICP-MS without applying an internal standard. *Chem Geol* 257(1):34–43
- Liu X-H, Xu J-W, Lai J-Q, Song X-F, He H-S, Zhang L-J, Shi J, Zhou X, Liao J, Cao Y-H, Li B (2023) Genetic significance of trace elements in hydrothermal quartz from the Xiangzhong metallogenic province South China. *Ore Geol Rev* 152:105229
- Luo K, Zhou J-X, Feng Y-X, Uysal IT, Nguyen A, Zhao J-X, Zhang JW (2020) In situ U–Pb dating of calcite from the South China antimony metallogenic belt. *iScience* 23(10):101575
- Ma DS, Liu YJ (1992) Geochemical characteristics and genesis of stratabound gold deposits in Jiangnan gold metallogenic belt. *Sci China Ser B* 35(2):240–256 (in Chinese with English abstract)
- Ma DS, Pan JY, Xie QL, He J (2002) Ore source of Sb(Au) deposits in Central Hunan: I. evidences of trace elements and experimental geochemistry. *Mineral Depos* 21(04):366–376 (in Chinese with English abstract)
- Ma DS, Pan JY, Xie QL (2003) Ore sources of Sb(Au) deposits in central Hunan:II. Evid Isot Geochem Mineral Depos 22(1):78–87 (in Chinese with English abstract)
- Ma DS, Pan JY, Yang RY (2005) Genesis and geochemistry of mid-low temperature hydrothermal deposits (Au–Sb–Hg) in South China. Springer, Berlin Heidelberg, Berlin, Heidelberg, pp 1153–1155
- Mo JF, Zhao XL, Zhu WQ, Li HT (2020) Metallogenic law and prospecting direction of coal-based graphite in Hunan Province. *Coal Geol Explor* 48(1):19–26 (in Chinese with English abstract)
- Palmer MR, Turekian KK (1986) 187Os/186Os in marine manganese nodules and the constraints on the crustal geochemistries of rhenium and osmium. *Nature* 319(6050):216–220
- Peng B, Frei R (2004) Nd–Sr–Pb isotopic constraints on metal and fluid sources in W–Sb–Au mineralization at Woxi and Liaojaping (Western Hunan, China). *Miner Depos* 39(3):313–327
- Peng JT, Hu RZ (2001) Carbon and oxygen isotope systematics in the Ikangshan giant antimony deposit, central Hunan. *Geol Rev* 47(01):34–41 (in Chinese with English abstract)
- Peng JT, Hu RZ, Lin YX, Zhao JH (2002) Sm–Nd isotope dating of hydrothermal calcites from the Xikuangshan antimony deposit. *Cent Hunan Chin Sci Bull* 47(13):1134–1137 (in Chinese with English abstract)
- Peng J-T, Hu R-Z, Burnard PG (2003a) Samarium–neodymium isotope systematics of hydrothermal calcites from the Xikuangshan antimony deposit (Hunan, China): the potential of calcite as a geochronometer. *Chem Geol* 200(1):129–136
- Peng JT, Hu RZ, Zhao JH, Fu YZ, Lin YX (2003b) Scheelite Sm–Nd dating and quartz Ar–Ar dating for Woxi Au–Sb–W deposit, western Hunan. *Chin Sci Bull* 48(23):2640–2646 (in Chinese with English abstract)
- Shah MT, Khan T, Khan A (2010) Lead isotope signatures of Pb–Zn sulfide mineralization in the Reshian–Lamnian area of Azad Jammu and Kashmir Pakistan. *Chinese J Geochem* 29(1):65–74
- Shirey SB, Walker RJ (1995) Carius tube digestion for low-blank rhenium–osmium analysis. *Anal Chem* 67(13):2136–2141
- Shu LS (2012) An analysis of principal features of tectonic evolution in South China block. *Geol Bull China* 31(7):1035–1053 (in Chinese with English abstract)
- Shu LS, Shi YS, Guo LZ (1995) The late proterozoic plate tectonics and collisional kinematics in the middle part of the Jiangnan Belt. Nanjing University Publishing House, Nanjing, 1–174 (in Chinese with English abstract)
- Sun JM, Luo YL, Gao LJ, Bao ZX (2007) Geology and metallogenesis of precambrian gold deposits in Central Hunan province. *Geol Resour* 16(3):189–195 (in Chinese with English abstract)
- Walker RJ, Morgan JW, Naldrett AJ, Li C, Fassett JD (1991) Re–Os isotope systematics of Ni–Cu sulfide ores, Sudbury igneous complex, Ontario: evidence for a major crustal component. *Earth Planet Sci Lett* 105(4):416–429
- Wang XQ, Longf XL, Zhao XL (2012a) Characteristics and coal resource prediction of carboniferous Ceshui formation in Central Hu’nan. *Coal Geol Explor* 40(6):8–12 (in Chinese with English abstract)

- Wang YL, Chen YC, Wang DH, Xu J, Chen ZH (2012b) Scheelite Sm-Nd dating of the Zhazixi W-Sb deposit in Hunan and its geological significance. *Geol China* 39(5):1339–1344 (in Chinese with English abstract)
- Wang FY, Ge C, Ning SY, Nie LQ, Zhong GX, Noel CW (2017a) A new approach to LA-ICP-MS mapping and application in geology. *Acta Petrologica Sinica* 33(11):3422–3436 (in Chinese with English abstract)
- Wang ZG, Wang KY, Wan D, Konare Y, Wang CY (2017b) Genesis of the Tianbaoshan Pb–Zn–Cu–Mo polymetallic deposit in eastern Jilin, NE China: Constraints from fluid inclusions and C–H–O–S–Pb isotope systematics. *Ore Geol Rev* 80:1111–1134
- Xiao X, Zhou T-F, White NC, Zhang L-J, Fan Y, Wang F-Y, Chen X-F (2018) The formation and trace elements of garnet in the skarn zone from the Xinqiao Cu-S-Fe-Au deposit, Tongling ore district, Anhui Province, Eastern China. *Lithos* 302–303:467–479
- Xu G (1998) Geochemistry of sulphide minerals at Dugald River, NW Queensland, with reference to ore genesis. *Mineral Petrol* 63(1–2):119–139 (in Chinese with English abstract)
- Xu ZG, Chen YC, Wang DH, Chen ZH, Li HM (2008) China mineralization area division scheme. Beijing: Geological Publishing House, Beijing, 1–138 (in Chinese with English abstract)
- Yang DS, Shimizu M, Shimazaki H, Li XH, Xie QL (2006a) Sulfur isotope geochemistry of the supergiant Xikuangshan Sb deposit, central Hunan, China: constraints on sources of ore constituents. *Resour Geol* 56(4):385–396
- Yang RY, Ma DS, Bao ZY, Pan JY, Cao SL, Xia F (2006b) Geothermal and fluid flowing simulation of ore-forming antimony deposits in Xikuangshan. *Sci China, Ser D Earth Sci* 49(8):862–871 (in Chinese with English abstract)
- Yuan MW, Li SR, Li CL, Santosh M, Alam M, Zeng YJ (2018) Geochemical and isotopic composition of auriferous pyrite from the Yongxin gold deposit, Central Asian Orogenic Belt: Implication for ore genesis. *Ore Geol Rev* 93:255–267
- Zartman RE, Doe BR (1981) Plumbotectonics—the model. *Tectonophysics* 75(1–2):135–162
- Zhai DG, Williamsjones AE, Liu JJ, Tombros S, Cook NJ (2018) Mineralogical, Fluid Inclusion, and Multiple Isotope (H–O–S–Pb) Constraints on the Genesis of the Sandaowanzi Epithermal Au–Ag–Te Deposit. *NE China Econ Geol* 113(6):1359–1382
- Zhai DG, Liu JJ, Cook NJ, Wang XL, Yang YQ, Zhang AL, Jiao YC (2019) Mineralogical, textural, sulfur and lead isotope constraints on the origin of Ag–Pb–Zn mineralization at Bianjiadayuan, Inner Mongolia. *NE China Miner Depos* 54(1):47–66
- Zhang WJ (1980) Characteristics of coal measures sedimentary paleostructure of the Ceshui formation in Central Hunan. *Coal Geol Explor* 03:16–23 (in Chinese with English abstract)
- Zhang LS, Peng JT, Hu AX, Lin FM, Zhang T (2014) Re–Os dating of molybdenite from Darongxi tungsten deposit in Western Hunan and its geological implications. *Mineral Depos* 33(01):181–189 (in Chinese with English abstract)
- Zhang LJ, Shao YJ, Lai JQ, Shi J, Xu ZB (2015) Analysis on ore-controlling alteration rocks and structures in the Baojinshan–Jinkengchong gold deposit. *Hunan Mineral Explor* 6(03):245–253 (in Chinese with English abstract)
- Zhang Y, Pan JY, Zhou QQ, Liu Y, Ma CJ, Hu CC, Zhong FJ, Zhou WT (2016) S and Pb isotopic constraints on the multi-metal (W–Cu–Mo–U) mineralization of Ziyunshan Intrusive Rocks. *Jiangxi Prov Geochim* 45(05):510–526 (in Chinese with English abstract)
- Zhang FF, Wang YH, Liu JJ, Wang JC (2018) Ore genesis and hydrothermal evolution of the Wulandele Mo deposit, Inner Mongolia, Northeast China: evidence from geology, fluid inclusions and H–O–S–Pb isotopes. *Ore Geol Rev* 93:181–199
- Zhang Y (2018) Ore-forming fluid evolution and Sb–Au–W metallogenesis in the central Hunan–Northwestern Jiangxi, South China. Nanjing: Najing University, 1–145 (in Chinese with English abstract)
- Zhao H-B, Zhang Y, Liu L (2021) Hydrothermal alteration processes in the giant Dahutang tungsten deposit, South China: implications from litho-geochemistry and mass balance calculation. *China Geol* 4(2):230–244
- Zhou XL, He YL, Liu HS (2017) Geological characteristics of coal and graphite in Hanpoao mining area in northern section of Lianshao coalfield of Hunan Province. *Coal Geol Explor* 45(1):9–13 (in Chinese with English abstract)
- Zhou ZK, Li H, Yonezu K, Imai A, Tindell T (2023a) In-situ trace elements and sulfur isotopic analyses of stibnite: Constraints on the genesis of Sb/Sb-polymetallic deposits in southern China. *J Geochem Explor* 247:107177
- Zhou ZK, Li H, Zhu HR, Ghaderi M, Ouyang LM (2023b) Geochronology and geochemistry of ore-hosted zircon reveal the genesis of typical Sb–(Au–W) deposits in South China. *Ore Geol Rev* 155:105358

Springer Nature or its licensor (e.g. a society or other partner) holds exclusive rights to this article under a publishing agreement with the author(s) or other rightsholder(s); author self-archiving of the accepted manuscript version of this article is solely governed by the terms of such publishing agreement and applicable law.